

Submitted: November 7, 2023

Revised: November 21, 2023

Accepted: December 26, 2023

# Influence of various friction stir processing (FSP) schemes on the microstructure and properties of AD31 aluminium alloy busbar

A.E. Medvedev<sup>1</sup> , V.V. Atroshchenko<sup>2</sup> , A.S. Selivanov<sup>2</sup> , A.R. Bogdanov<sup>1</sup> , M.V. Gorbatkov<sup>3</sup> ,  
Y.V. Logachev<sup>2</sup> , V.S. Lobachev<sup>2</sup> 

<sup>1</sup> Ufa University of Science and Technology, Ufa, Russia

<sup>2</sup> LLC Attestation Center Svarka Tech. Service, Ufa, Russia

<sup>3</sup> LLC Krus-Zapad, Ufa, Russia

✉ medvedevandreyrf@gmail.com

## ABSTRACT

This paper examines the influence of various schemes for implementing friction stir processing (FSP) on the microstructure and properties of a conductive busbar made of AD31T (AA6063) aluminum alloy. In particular, the implementation of five different FSP schemes on the formation of structure and volumetric defects in the volume of the stir zone was studied. It has been shown that performing FSP at a tool rotation speed of 1120 rpm and a linear tool movement velocity of 200 mm/min ensures the absence of macroscopic defects in the volume of the stir zone. The implementation of certain FSP schemes made it possible to achieve the formation of an ultrafine-grained structure both in the near-surface layer and in the bulk of the material under study. This type of processing can be recommended as a way to increase the strength of aluminum materials without significant loss of their electrical conductivity.

## KEYWORDS

friction stir processing • FSP • Al-Mg-Si • AA6063 • aluminium alloy • fine-grained structure  
microhardness • electrical conductivity

**Acknowledgements.** *The authors express special gratitude to the Center for Collective Use "Nanotech" of the Federal State Budgetary Educational Institution of Higher Education "UUST".*

**Citation:** Medvedev AE, Atroshchenko VV, Selivanov AS, Bogdanov AR, Gorbatkov MV, Logachev YV, Lobachev VS. Influence of various friction stir processing (FSP) schemes on the microstructure and properties of AD31 aluminium alloy busbar. *Materials Physics and Mechanics*. 2024;52(1): 95-107. [http://dx.doi.org/10.18149/MPM.5212024\\_9](http://dx.doi.org/10.18149/MPM.5212024_9)

## Introduction

Aluminium and aluminium alloys occupy a significant share in the modern metallurgical industry. Along with relative availability, one of the most important properties of aluminium alloys that determine its widespread use is its low density and good electrical conductivity, accounting for 62 % of the electrical conductivity of copper. Considering the scarcity and high cost of copper, the role of aluminium as a conductor material is steadily increasing. The undoubted advantages of aluminium include its high plasticity, thermal conductivity and heat capacity, good manufacturability, and corrosion resistance [1]. The main disadvantage of aluminium is its relatively low strength - 49 MPa. This level of properties is not sufficient for widespread industrial use, so research aimed at increasing the strength of aluminium alloys is important. One of the ways to strengthen aluminium is to create alloys based on it [2]. The general pattern of aluminium alloying is that the

addition of other elements, leading to an increase in the strength of the aluminium alloy, leads to a decrease in its electrical conductivity [3–5]. The need to maintain the level of electrical conductivity of pure aluminium, or to minimize its drop due to alloying, as well as the desire to reduce the cost of production of aluminium alloys, lead to minimizing the amount of additions of alloying elements without a significant loss in properties - the creation of the so-called low-alloyed alloys [6,7].

Another fundamental approach to increasing the strength of aluminium and aluminium alloys is the use of deformation methods - stamping, drawing, pressing, etc. [2]. Such methods have undoubted advantages - they are well-developed modes and conditions of deformation, stability and predictability of the results obtained. The disadvantages of such methods include the volumetric nature of the impact - deformation, as a rule, extends to the entire volume of the processed material, as well as an increase in the density of defects, which entails a drop in electrical conductivity [8]. The effect of deformation can be reduced by using local hardening methods, such as cold-working, shot peening, diamond burnishing and other similar methods [1]. A separate group of methods aimed at modifying the surface and surface layer of a material includes methods based on the effect of surface friction. These include, in particular: friction stir welding, friction stir processing, friction surfacing, friction brazing, friction transformation hardening, friction extrusion and others [9]. The most popular and commonly used in industry are friction stir welding (FSW) and friction stir processing (FSP).

Friction stir processing (FSP) is a technology aimed at changing the structure and properties of the surface and subsurface layer of materials in the solid phase [9–11]. A distinctive feature of this method is local mixing of the metal in the treated area without the formation of a liquid phase, which can lead to oxidation and burnout of the metal, as well as a decrease in its strength properties. Work aimed at studying FSP quickly showed that this method can modify the surface layer of the processed material, providing a structure and properties different from the processed material [12]. Since FSP involves processing the material in the solid phase, the main attention has been paid to soft materials, such as aluminium alloys [13], magnesium alloys [14] and copper alloys [15]. There is also a limited set of publications on FSP of titanium alloys and steels [11,16].

Research aimed at FSP of aluminium alloys aims to create permanent joints where welding is not applicable or impractical. Thus, it was shown that FSP with the imposition of tracks on the aluminium surface makes it possible to reduce the average grain size to 100–200 nm over a relatively large area, reaching an ultrafine-grained (UFG) state [17–19]. The authors propose a similar approach that makes it possible to obtain large-sized products with a UFG structure of the surface layer. The authors of [13] claim a decrease in the average grain size per one pass of FSP by more than 20 times, which led to an increase in the yield strength of the material by 2.4 times. Articles [20–22] explore methods of friction stir welding with overlap, a two-pass connection in one direction and in opposite directions, on both sides of the welded sample. These studies claim that such methods can provide good fluidity and mixing of dissimilar metals, reducing the size of grains and defects at their boundaries, and a two-pass connection can significantly increase the strength properties of the welded joint, reduce wear, and obtain minimal costs for mixing tools.

Despite a large amount of information regarding the FSP of aluminium alloys, there is depressingly little data on the effect of this processing method on the electrical conductivity of aluminium alloys. There is no data on the effect of this processing method on the level of electrical conductivity in conductive products made from aluminium alloys. This study is a continuation of works devoted to the FSP of conductive busbars made of aluminium alloy AD31 [23]. In previous work, a rational FSP mode was established, which allows, for a given geometry of the processing tool, to obtain a processed zone without volumetric defects. This paper examines five different schemes for implementing FSP, their influence on the structure and properties of busbars made of AD31T aluminium alloy.

## Materials and Methods

As a research material, hot-rolled aluminium alloy plates of 10 mm thick and 200 × 200 mm in size were used. The plates were obtained in the "T" state, meaning quenching and natural aging. The chemical composition of the commercially produced AD31T alloy (AA6063 analogue) is given in Table 1.

**Table 1.** Chemical composition of the AD31T alloy

Concentration of the element, wt. %						
Al	Si	Fe	Mg	Mn	Cu	Zn
Base material	0.410	0.390	0.390	≤ 0.035	≤ 0.035	≤ 0.035

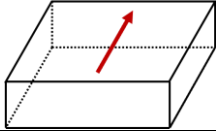
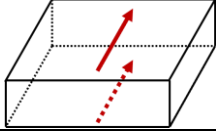
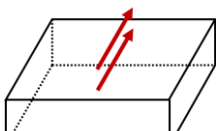
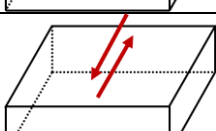
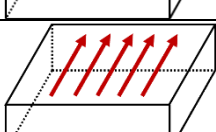
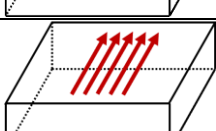
The processing of the material was carried out on a vertical console milling machine FSS-400, adapted for FSP, in 6 different processing schemes (Table 2). Based on the results of previous research [23], the FSP parameters were set as follows: tool rotation speed 1120 rpm, tool linear velocity 200 mm/min. During FSP, the shoulder penetration was 0.635 mm at a tool inclination angle of 3°. The tool dwelling time after immersion is 10 sec.

A sketch of the tool is shown in Fig. 1. The tool is made of steel containing 0.2 wt. % C and 13 wt. % Cr (the closest analogue is AISI 420). Before use, the tool is hardened up to 580 HB. Most authors tend not to disclose the details of the geometry of the stirring tool, however, the general recommendations for aluminium alloys are that the tool pin should be a tapered cone or a threaded one. Since the production of the threaded tool is more expensive and complex, than the production of the tapered cone tool, and tapered cone tool is proven to provide defect less structure [22,24,25], the latter type of tool was used.



**Fig. 1.** Schematic drawing of the stirring tool

**Table 2.** FSP schemes

Marking of the sample	FSP scheme description	FSP scheme depiction
225	Single linear track	
226	Two unidirectional tracks, on a single line, one from each surface (upper and lower) of the plate	
227	Two unidirectional tracks, on a single line, on top of each other, on the same surface of the plate	
228	Two counter directional tracks, on a single line, on top of each other, on the same surface of the plate	
229	Multiple unidirectional overlapping tracks on the same surface, overlap of 10 mm	
233	Multiple unidirectional overlapping tracks on the same surface, overlap of 5 mm	

X-ray control was carried out on the hardware-software complex of digital radiography "Tsifrakon". Microstructure studies were performed on an Olympus Q150R optical microscope. For metallographic analysis, macrosections were made by cutting in the middle of the length of the stir zone (SZ) in the direction perpendicular to the processing direction. Surface finishing was carried out in a 3 % hydrofluoric acid solution to reveal the macrostructure. Microhardness (HV) was evaluated by the Vickers method on a Buehler MicroMet 5101 instrument at a load of 1 N and a holding time under load of 10 s. The microhardness (HV) value was calculated using the Omnimet Imaging System software. Microhardness was measured on transverse sections of specimens along lines parallel to the surface of the original plate. The measurements were taken at the middle of the sample thickness, and  $\frac{1}{4}$  of the height from the bottom and top surfaces of the plate. When measuring the microhardness of the stir zone, the line of measurements passed through all sections of the cross-section of the FSP sample at a measurement step of 0.5 mm (about 60 measurements per line). The error value for the microhardness profiles was calculated as a standard deviation for each profile. Generally, the absolute value of the microhardness error does not exceed 5 HV. Mechanical tensile tests were carried out on samples manufactured in accordance with GOST 1497-84. Tests were carried out on flat samples with length 70 mm and cross-sectional dimensions 3 × 9 mm. The samples were cut in the direction perpendicular to the FSP treatment so that the treated area aligned with the middle of the sample. Specific electrical conductivity ( $\omega$ ) of the alloy samples was determined with a relative error of 2% using a VE-27NTs/4-5 eddy

current electrical conductivity meter according to ASTM E1004-09. The electrical conductivity value of the samples relative to annealed copper (International Annealed Copper Standard) was calculated using Eq. (1):

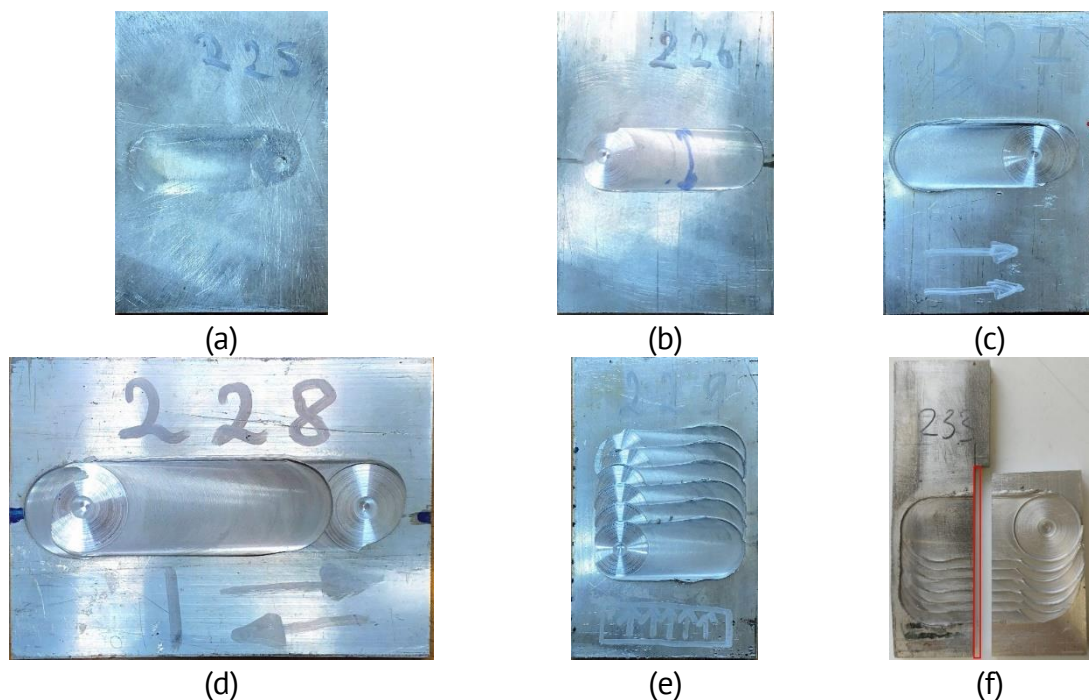
$$IACS = \omega_{Al} / \omega_{Cu} \cdot 100 [\%], \quad (1)$$

where  $\omega_{Al}$  is the experimentally determined value of the electrical conductivity of the aluminium alloy sample,  $\omega_{Cu}$  is the electrical conductivity of annealed copper, equal to 58 MS/m, (MS/m stands for  $10^6$  S/m, siemens per meter). Since the electrical conductivity was measured at 10 points on a line located in the middle of the sample thickness.

## Results and Discussion

### Samples and stir zone (SZ) assessment

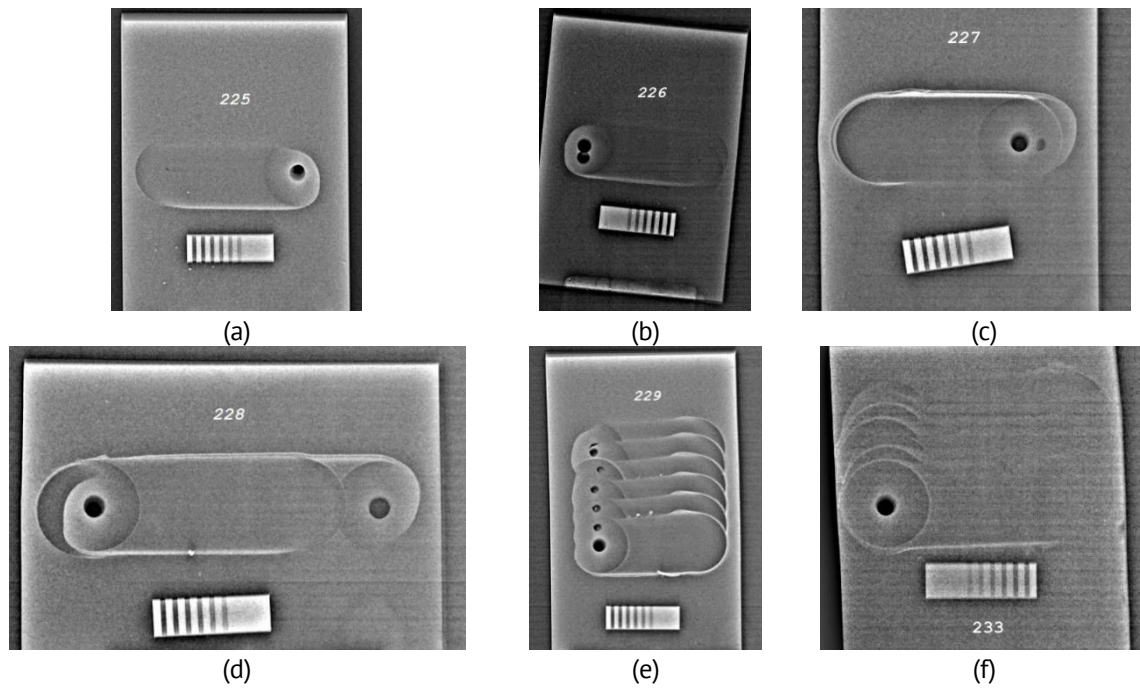
Images of the samples 225-233 are presented on Fig. 2. Sample 225 was produced to ensure the correctness of the chosen FSP mode [23] in appliance to the studied material, ensuring the absence of macroscopic defects in the research material. Visual attestation of the samples 226-233 shows the absence of the macroscopic defects, tunnel effect, melting and excessive material pushouts from the stir zone during FSP. Figure 2(f) on example of 233 demonstrates the placement of the tensile test samples.



**Fig. 2.** Samples 225(a), 226 (b), 227 (c), 228 (d), 229 (e) and 233 (f) after FSP. Red rectangle on (f) represents the placement of the tensile test sample

The results of X-ray control of samples 225–229 and 233 are presented in Fig. 3. Each of the studied samples demonstrate the absence of the volumetric defects: tunnel defects, gas pores and other.

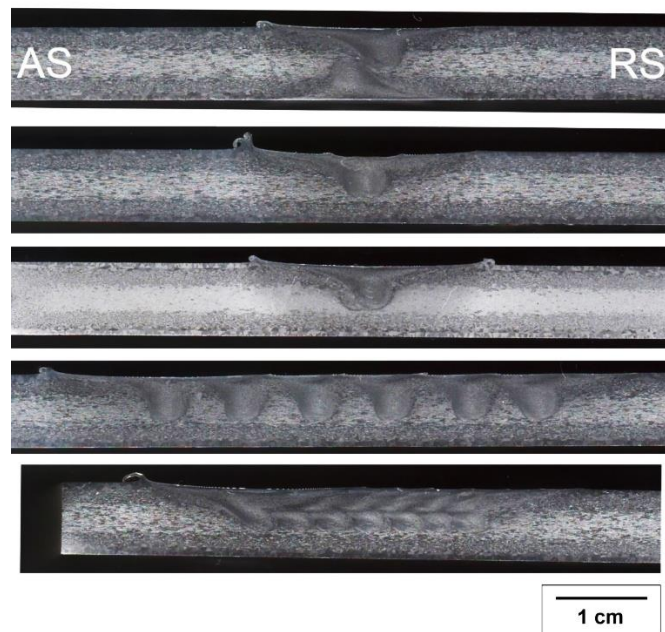
Since sample 225 was used as a reference one for testing the FSP conditions, it was no longer studied further.



**Fig. 3.** Results of the X-Ray control of samples 225 (a), 226 (b), 227 (c), 228 (d), 229 (e) and 233 (f) after the FSP

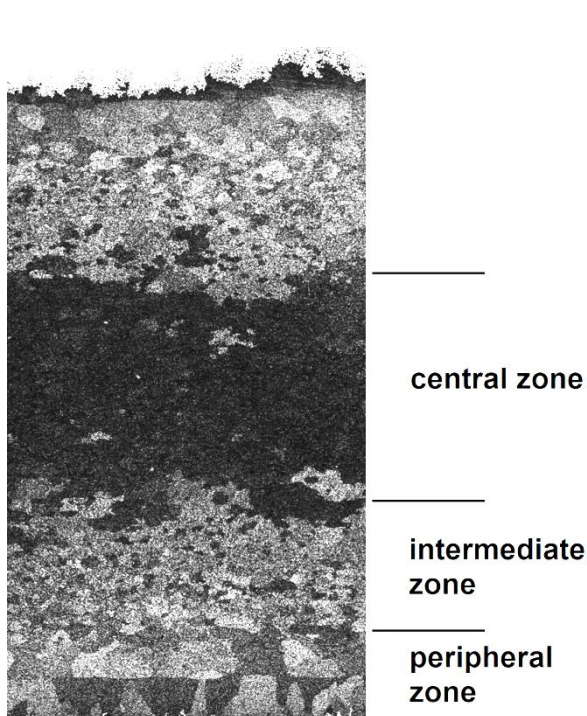
### Macrostructure assessment

Figure 4 shows photographs of the cross-section of samples 226-233 after FSP. As a result of FSP, a finely dispersed structure was formed in the stir zone (SZ) and the heat affected zone (HAZ) (Fig. 4). The shape and size of the HAZ is similar for samples 227–229 - it narrows towards the base of the sample due to more significant heat dissipation in the sample volume. The HAZ of samples 229 and 233 is wider than in samples 226-228 due to the overlap of the HAZ of each individual track.



**Fig. 4.** Macrostructure assessment of the 226 - 233 samples (top to bottom) cross-sections. Advancing side and retreating side are marked AS and RS, correspondingly

According to macroscopy data, a busbar made of the alloy under study in the initial state is characterized by three zones - central, intermediate, and peripheral (Fig. 5). The central zone is characterized by relatively small, elongated grains with the size not exceeding  $100\ \mu\text{m}$ . In the intermediate zone, grains are characterized by a larger size, ranging from  $50$  to  $300\ \mu\text{m}$  with an average of  $146\ \mu\text{m}$ , and a shape close to equiaxial. The peripheral zone consists of coarse crystals arranged in 1 or 2 rows. These coarse grains are generally presented in the shape of elongated towards the edge of the busbar grains, with the average length of  $337\ \mu\text{m}$  (ranging from  $130$  to  $740\ \mu\text{m}$ ) and average width of  $571\ \mu\text{m}$  (ranging from  $300$  to  $900\ \mu\text{m}$ ).



**Fig. 5.** Macroscopic images of the initial busbar cross section. Three zones are distinctly visible – central, intermediate, and peripheral, OM

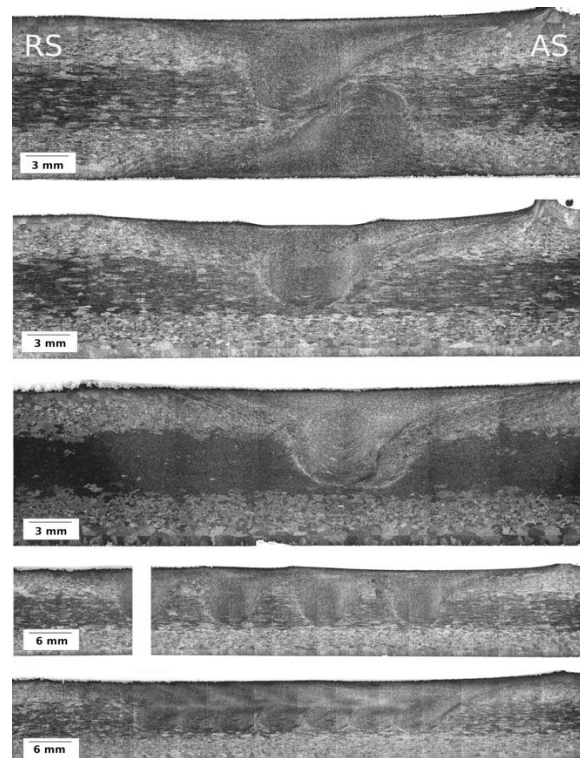


**Fig. 6.** Metallographic analysis of the samples 226-233 cross sections (top to bottom), OM. Advancing side and retreating side are marked AS and RS, correspondingly

Figure 6 presents the panoramic images of the 226-233 samples. According to it, the grain size within the SZ ranges from  $20$  to  $30\ \mu\text{m}$  with an average of  $22 \pm 8\ \mu\text{m}$ . The value of the average grain size is the same throughout the SZ, so the deformation could be considered uniform in the SZ. Outside the SZ, however, in the HAZ the average size of the grain is  $295.35\ \text{nm}$ , which is higher than in both intermediate and central zones of the busbar (Fig. 5). The grain growth presumably is caused by the heating inevitably accompanying the FSP process.

According to Fig. 6, in sample 226, the tracks located on different sides of the busbar did superimpose each other but were located offset. However, the SZs of both tracks influenced each other, bending the normally symmetrical shape of the SZ. In samples 227 and 228, the tracks overlapped with virtually no displacement relative to each other. If in sample 227 the directions of tool movement coincided, and the advancing side (AS) and

retreating side (RS) zones overlapped each other, increasing the heterogeneity of the thermomechanically affected zone (TMAZ), then in sample 228, during the second pass, the AS and RS zones overlapped each other, providing a symmetrical TMAZ. Sample 229 was obtained with superimposed unidirectional tracks with a tool offset of 10 mm. As it turned out, a displacement of this magnitude does not provide only partial overlap of the SZ, leaving untreated areas. In sample 233, processed according to a scheme similar to sample 229, the displacement of the tracks was 5 mm, as a result of which complete overlap of the SZ was achieved.

### **Microhardness and electrical conductivity assessment**

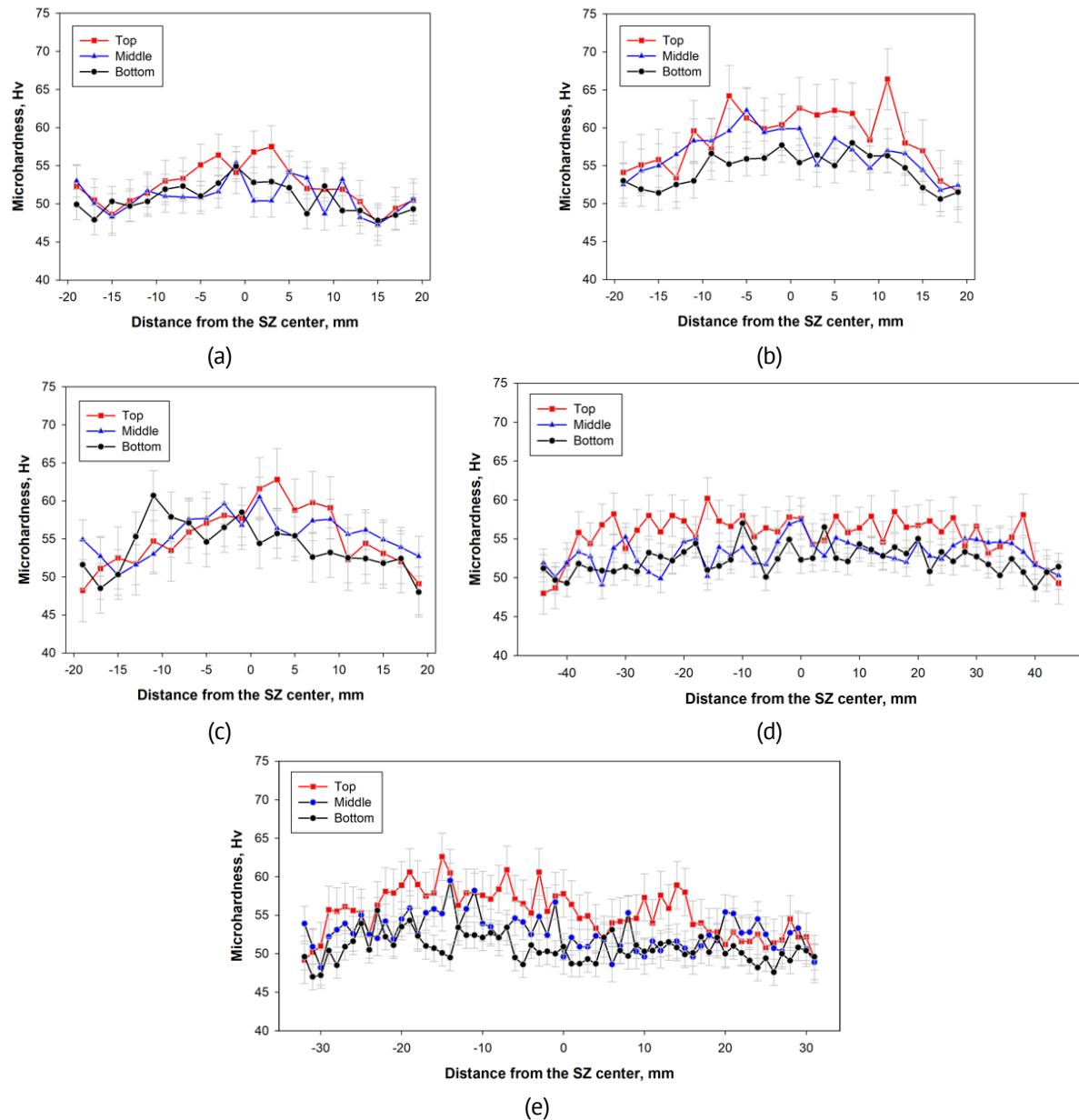
Analysis of the hardness distribution curves (Fig. 7) shows that the cross-section of sample 226 is characterized by two significantly different sections: the base metal (BM), which hardness is 50-55 HV (depending on the depth of measurements relative to the surface), and the metal of the SZ, the hardness of which is on average 10–15 % higher. There is also a noticeable decrease in hardness at the boundary of the SZ, between the BM and the TMAZ, caused by recovery processes as a result of thermal effects. Microhardness values increase in the center of the SZ, since due to a greater degree of deformation, the contribution of grain boundary and dislocation strengthening increases as well.

The microhardness profiles of samples 226-228 are largely similar, however, there are certain differences. In sample 226, there was no exact overlap of the SZ core, as a result of which the TMAZ of the second track partially overlapped the SZ core of the first track, leading to softening - the maximum microhardness in sample 226 does not reach 60 HV, which is the minimum value for samples 226-228 (Fig. 7(a)). The microhardness values for the upper, middle, and lower zones of the sample are almost completely identical, which indicates the absence of hardening in the surface zone. Also, the microhardness values completely coincide in the center of the sample - between the centers of the SZ cores.

In sample 227, in which unidirectional tracks were superimposed, an increase in microhardness is observed throughout the entire SZ and TMAZ, and the hardness values for the upper and middle layers of the sample turned out to be higher than for the lower layer (Fig. 7(b)). The multidirectionality of the tracks in sample 228 caused the strengthening of the lower layer, in addition to an increase in microhardness in the upper and middle layers of the sample (Fig. 7(c)). In general, the increase in microhardness in sample 228 is less pronounced, most likely due to the overlap of the HAZ from multidirectional tool passes.

The nature of the microhardness profiles for samples 229 and 233 is different from samples 226-228. In sample 229, the microhardness of the surface layer turned out to be higher than in the base material, since the overlap of the SZ core is located just near the surface. The microhardness of the lower layer of the busbar increases slightly, but the change is insignificant. The microhardness profile of the middle layer has a sawtooth character, corresponding to alternating SZs (Figs. 4-6). The growth of microhardness in the upper and middle zones of sample 233 is more pronounced than in sample 229, and, in general, the hardening in sample 233 is greater than in sample 229. A characteristic feature of sample 233 is a sharp decrease in microhardness at the boundary of the zone - where the overlaps of the SZs, and this decrease is most noticeable in the upper and middle layers of the sample.





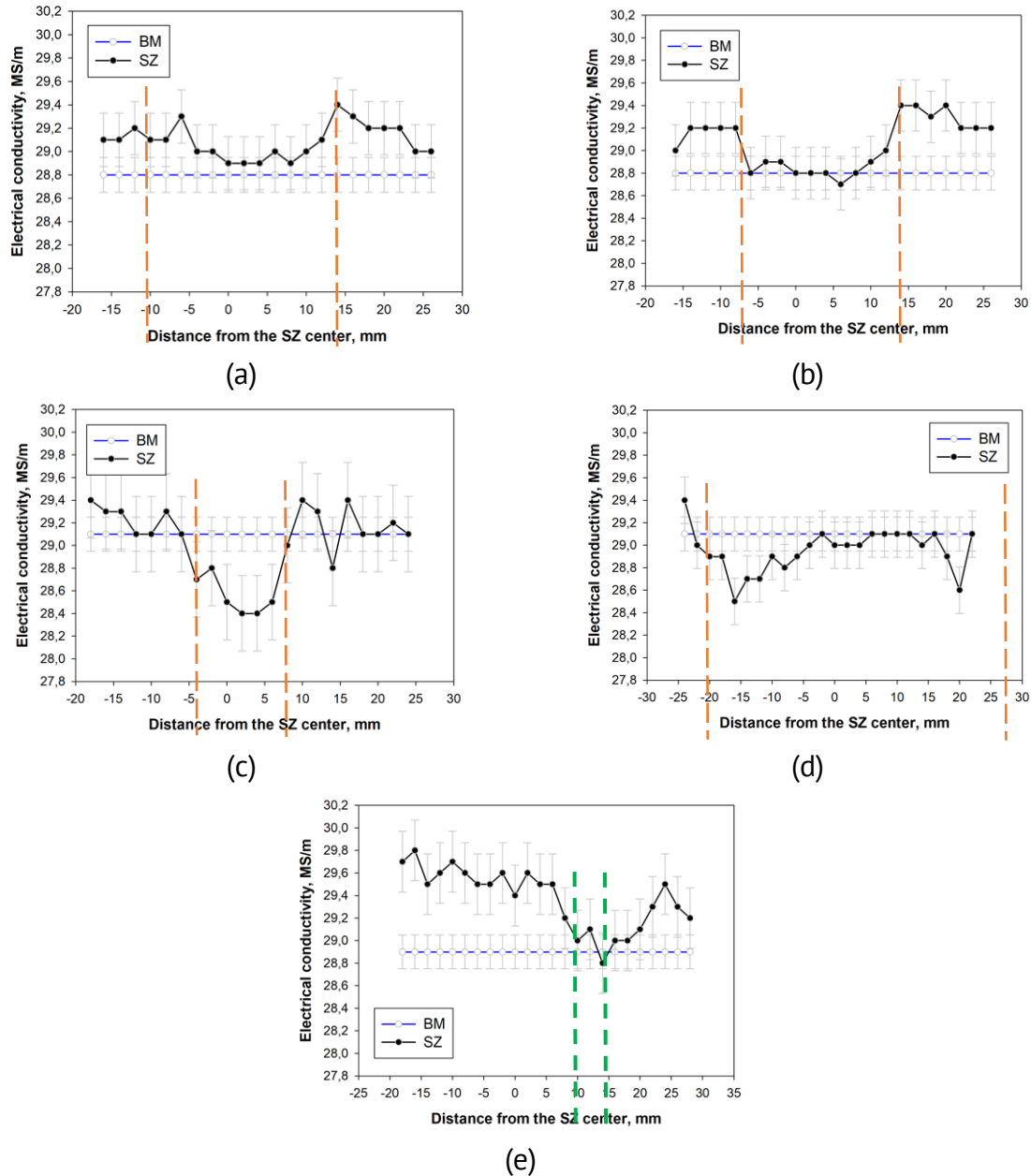
**Fig. 7.** Microhardness profiles for the samples 226 (a), 227 (b), 228 (c), 229 (d) and 233 (e). For all samples advancing side (AS) is on the right and retreating side (RS) is on the left

Figure 8 shows the electrical conductivity profiles of the samples. Based on the results of measuring the electrical conductivity of the SZ and TMAZ, the average value of the electrical conductivity of the BM was 28.8–29.1 MS/m.

The change in resistivity value for each sample is different from the others. Thus, in sample 226, there is a noticeable decrease in electrical conductivity in the SZ and TMAZ (Fig. 8(a)), and an increase beyond them. According to Fig. 8(a), a relatively small increase in microhardness is observed in the sample SZ, which correlates with a decrease in electrical conductivity. Near the SZ, an increase in electrical conductivity is observed, probably as a result of recovery processes. The behavior of electrical conductivity in samples 227 and 228 correlates with changes in microhardness - for example, the microhardness in the SZ of sample 227 is higher, and the electrical conductivity is lower than in the SZ of sample 228. The electrical conductivity values to the left and right of

the SZ and TMAZ in sample 228 are higher than in sample 227 are and are located symmetrically due to the overlap of the AS and RS zones from each tool pass.

Just like microhardness, the electrical conductivity profiles in samples 229 and 233 are different from the electrical conductivity profiles for samples 226-228. In general, the electrical conductivity of the TMAZ of the sample 229 corresponds to the electrical conductivity of the BM, except for areas at the edge of the SZ. The electrical conductivity of sample 233 is higher almost throughout its entire length than in the base material, and decreases only at the edge of the SZ (Fig. 8(f)).



**Fig. 8.** Electrical conductivity profiles for samples 226 (a), 227 (b), 228 (c), 229 (d) and 233 (e). Orange dashed lines mark the edges of the SZ. For the sample 233 (e) green dashed lines mark the start and the end of the SZ edge. For all samples advancing side (AS) is on the right and retreating side (RS) is on the left

Figure 9 shows the engineering stress-strain curves of samples made from workpieces of states 226–233. All states are characterized by ductile fracture and have comparable values of the yield strength (UTS) (70–80 MPa), ultimate tensile strength (140–160 MPa) and ductility (16–18 %). The sawtooth sections of the tensile curves indicate alternating localization of deformation and its relaxation.

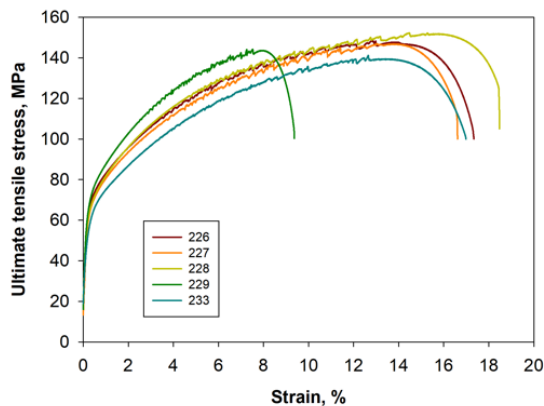


**Fig. 9.** Engineering strain-stress curves for the 226-233 samples



**Fig. 10.** Fractures tensile tests samples of the 226-233 (top to bottom) samples

Figure 10 presents the fractured tensile test samples of the 226-233 states. Judging by these images, all samples failed outside the FSP region. Firstly, this indicates the strengthening effect of FSP, and secondly, the absence of defects introduced by FSP. On samples 226, 227 and 228 it is clearly visible that the localization of deformation occurred on both sides of the SZ. The wavy relief of localized deformation zones confirms the assumption of alternating localization and relaxation of deformation during tensile tests.

In this study, the implementation of various FSP schemes was carried out for two purposes: the first group of samples (226–228) was obtained for the purpose of testing the linear FSP regime, the second (229, 233) was obtained for the purpose of modifying the structure and properties in a certain volume of the sample. It is known that during FSP a number of processes might occur: plastic deformation, recovery, static and dynamic recrystallization, formation and decomposition of a solid solution, phase transformations [25–28]. All or some of these processes can occur simultaneously, forming different structures in the section of the SZ and TMAZ. However, judging by the results of the study, processes aimed at increasing the mechanical strength in the SZ predominate in the modes used. Despite the fact that in aluminium alloys an increase in electrical conductivity and electrical conductivity are considered competing properties [29], in this case it was possible to achieve an increase in microhardness (Fig. 7) and ultimate tensile strength (Fig. 9) in the SZ without a decrease, and in some cases - with increasing the electrical conductivity (Fig. 8). The results allow us to assert that for alloys of the Al-Mg-Si system (possibly for other thermally hardenable aluminium alloys as well), the given FSP processing modes allow obtaining a defect-free linear processing zone characterized by increased hardness, strength and electrical conductivity relative to the base material (226–228), as well as modifying a volume of material of a certain depth, which is also characterized by increased hardness, strength and electrical conductivity relative to the base material (229, 233).

## Conclusions

In this work, five FSP schemes were implemented, three of them along a line, two along a surface, in the same process conditions: linear tool velocity of 200 mm/min and tool rotation speed of 1120 rpm. The authors have drawn the following conclusions:

1. Proposed FSP schemes implemented on a 10 mm thick conductive busbar made of commercial aluminium alloy AD31T (Al-Mg-Si system, analogue of AA6063) provided a defect-free structure.
2. Due to the implementation of each scheme in the volume of the treated area, due to plastic deformation, a decrease in the average grain size occurred, accompanied by hardening and a decrease in electrical conductivity. In thermally affected areas, located on the periphery of the stir zone, reverse processes occurred.
3. During mechanical tests, the destruction of samples of all proposed FSP schemes occurred outside the FSP zone, accompanied by alternating localization and relaxation of deformation.
4. Based on the research carried out, to create permanent connections of conductive aluminium busbars, it is recommended to use scheme 227 (parallel unidirectional passes with complete overlap of the second pass on the first), for strengthening treatment of the surface and near-surface layer – scheme 233 (parallel unidirectional passes of the tool, with overlapping tracks by 5 mm – at a given tool configuration).

## References

1. Polmear I, StJohn D, Nie JF, Qian M. *Light Alloys: Metallurgy of the Light Metals*. 5th ed. Butterworth-Heinemann; 2017.
2. Verma RP, Kumar Lila M. A short review on aluminium alloys and welding in structural applications. *Mater. Today Proc.* 2021;46: 10687–10691.
3. Valiev RZ, Murashkin M, Sabirov I. A nanostructural design to produce high-strength Al alloys with enhanced electrical conductivity. *Scr. Mater.* 2014;76: 13–16.
4. Murashkin MY, Sabirov I, Medvedev AE, Enikeev NA, Lefebvre W, Valiev RZ, Sauvage X. Mechanical and electrical properties of an ultrafine grained Al-8.5wt. % RE (RE=5.4wt.% Ce, 3.1wt.% La) alloy processed by severe plastic deformation. *Mater. Des.* 2016;90: 433–442.
5. Orlova TS, Mavlyutov AM, Bondarenko AS, Kasatkin IA, Murashkin MY, Valiev RZ. Influence of grain boundary state on electrical resistivity of ultrafine grained aluminium. *Philosophical Magazine*. 2016;96(23): 2429–2444.
6. Belov N, Murashkin M, Korotkova N, Akopyan T, Timofeev V. Structure and properties of Al-0.6 Wt.%Zr wire alloy manufactured by direct drawing of electromagnetically cast wire rod. *Metals*. 2020;10(6): 769.
7. Belov N, Akopyan T, Korotkova N, Murashkin M, Timofeev V, Fortuna A. Structure and properties of ca and zr containing heat resistant wire aluminum alloy manufactured by electromagnetic casting. *Metals*. 2021;11(2): 236.
8. Murashkin MY, Sabirov I, Sauvage X, Valiev RZ. Nanostructured Al and Cu alloys with superior strength and electrical conductivity. *J. Mater. Sci.* 2016;51(1): 33–49.
9. Nicholas ED. Friction Processing Technologies. *Welding in the World*. 2003;47(11): 2–9.
10. Mishra RS, De PS, Kumar N. Friction Stir Processing. In: *Friction Stir Welding and Processing*. Cham: Springer; 2014. p.259–296.
11. Ma ZY. Friction stir processing technology: A review. *Metall. Mater. Trans. A*. 2008;39: 642–658.
12. Kurt A, Uygur I, Cete E. Surface modification of aluminium by friction stir processing. *J. Mater. Process. Technol.* 2011;211(3): 313–317.
13. Yadav D, Bauri R. Effect of friction stir processing on microstructure and mechanical properties of aluminium. *Materials Science and Engineering A*. 2012;539: 85–92.
14. Wang W, Han P, Peng P, Zhang T, Liu Q, Yuan SN, Huang LY, Yu HL, Qiao K, Wang KS. Friction Stir Processing of Magnesium Alloys: A Review. *Acta Metall. Sin. (Engl. Lett.)*. 2020;33: 43–57.
15. Isa MSM, Moghadasi K, Ariffin MA, Raja S, bin Muhamad MR, Yusof F, Jamaludin MF, Yusoff NB, Ab Karim S, Recent research progress in friction stir welding of aluminium and copper dissimilar joint: a review. *Journal of Materials Research and Technology*. 2021;15: 2735–2780.
16. Hajian M, Abdollah-Zadeh A, Rezaei-Nejad SS, Assadi H, Hadavi SMM, Chung K, Shokouhimehr M. Microstructure and mechanical properties of friction stir processed AISI 316L stainless steel. *Mater. Des.* 2015;67: 82–94.

17. Su JQ, Nelson TW, Sterling CJ. Friction stir processing of large-area bulk UFG aluminum alloys. *Scr. Mater.* 2005;52(2):135–140.
18. Su JQ, Nelson TW, Sterling CJ. Microstructure evolution during FSW/FSP of high strength aluminum alloys. *Materials Science and Engineering A.* 2005;405(1–2): 277–286.
19. Su JQ, Nelson TW, Sterling CJ. A new route to bulk nanocrystalline materials. *J. Mater. Res.* 2003;18(8): 1757–1760.
20. Liyakat NA, Veeman D. Improvement of mechanical and microstructural properties of AA 5052-H32 TIG weldment using friction stir processing approach. *Journal of Materials Research and Technology.* 2022;19: 332–344.
21. Sharma V, Gupta Y, Kumar BVM, Prakash U. Friction Stir Processing Strategies for Uniform Distribution of Reinforcement in a Surface Composite. *Materials and Manufacturing Processes.* 2016;31(10): 1384–1392.
22. Sarmadi H, Kokabi AH, Seyed Reihani SM. Friction and wear performance of copper-graphite surface composites fabricated by friction stir processing (FSP). *Wear.* 2013;304(1–2): 1–12.
23. Medvedev AE, Atroshchenko VV, Selivanov AS, Bogdanov AR, Gorbatkov MV, Logachev YV, Lobachev VS, Sadrislamov AR. The influence of friction stir processing on the microstructure and properties of the AD31T alloy. *Materials Physics and Mechanics.* 2023;51(4): 38–49.
24. Memon S, Paidar M, Ojo OO, Cooke K, Babaei B, Masoumnezhad M. The role of stirring time on the metallurgical and mechanical properties during modified friction stir clinching of AA6061-T6 and AA7075-T6 sheets. *Results Phys.* 2020;19: 103364.
25. Wakchaure K, Thakur A. Mechanical and microstructural characteristics of underwater friction stir welded AA 6061-T6 joints using a hybrid GRA-artificial neural network approach. *Materials Physics and Mechanics.* 2023;51(1): 119–141.
26. Soleymani S, Abdollah-Zadeh A, Alidokht SA. Microstructural and tribological properties of ultra fine grained hybrid composite produced by friction stir processing. *Materials Physics and Mechanics.* 2013;17: 6–10.
27. Lebaal N, Chamoret D, Schlegel D, Folea M. Thermal modelling of friction stir process (FSP) and identification parameters. *Materials Physics and Mechanics.* 2017;32: 14–20.
28. Mimmi A, Merzoug M, Ghazi A, Dellal N. Mechanical behavior of structures welded with friction stir lap welding process. *Materials Physics and Mechanics.* 2023;51(2): 151–163.
29. GENC M, Eloi P, Blandin JJ, Pascal C, Donnadiou P, De Geuser F, Lhuissier P, Desrayaud C, Martin G. Optimization of the strength vs. conductivity trade-off in an aluminium alloy designed for laser powder bed fusion. *Materials Science and Engineering: A.* 2022;858: 144139.

## About Authors

**Andrey E. Medvedev**  

*Candidate of Physical and Mathematical Sciences*

*Senior Researcher (Ufa University of Science and Technology, Ufa, Russia)*

**Valery V. Atroshchenko**  

*Doctor of Technical Sciences*

*Head of Chair of Modern Methods of Welding and Structural Control (LLC Attestation Center Svarka Tech. Service, Ufa, Russia)*

**Aleksey S. Selivanov**  

*Candidate of Technical Sciences*

*Head of Scientific and Technical Department (LLC Attestation Center Svarka Tech. Service, Ufa, Russia)*

**Albert R. Bogdanov**

*Bachelor Student (Ufa University of Science and Technology, Ufa, Russia)*

**Mikhail V. Gorbatkov**  

*Engineer (LLC Krus-Zapad, Ufa, Russia)*

**Yury V. Logachev**  

*Head of Research and Development Institute (LLC Attestation Center Svarka Tech. Service, Ufa, Russia)*

**Vladislav S. Lobachev**  

*Engineer (LLC Attestation Center Svarka Tech. Service, Ufa, Russia)*